Spin-state determinations and spacings of neutron resonances for ^{187}Os and ^{189}Os†

A. Stolovy* and A. I. Namenson
Naval Research Laboratory, Washington, D. C. 20375

B. L. Berman
Lawrence Livermore Laboratory, University of California, Livermore, California 94550

(Received 15 March 1976)

The spin states of 25 resonances for (^{187}Os + n) and 40 resonances for (^{189}Os + n) have been determined with probabilities of correctness greater than 80%. Spin assignments were made on the basis of the ratios of low-energy γ-ray intensities associated with neutron capture in the resonances. For both nuclei, the spin distributions are consistent with a $(2J+1)$ level-density distribution. The level spacings favor the theory of Dyson and Mehta, but an uncorrelated Wigner distribution cannot be ruled out definitely. These results provide important input parameters for the astrophysical determination of the age of the universe by the ^{187}Re$\rightarrow$^{187}Os nuclear dating technique.

[NUCLEAR REACTIONS ^{187,189}Os(n,γ), $E=5$–350 eV, enriched targets; measured E_n, E_γ, I_γ; deduced $J, \Delta_3, \langle D\rangle$.]

I. INTRODUCTION

There has been much interest recently in the osmium isotopes, especially with respect to (a) the study of nucleocosmochronology by means of the β decay of ^{187}Re to ^{187}Os (with a half-life of $\sim 5\times10^{10}$ years), in order to determine the age of the universe[1] and (b) the possibility of a phase transition in nuclear shape and stability.[2] For the astrophysical problem, one needs to know both the total neutron-capture cross sections as a function of neutron energy and the spin-state distributions and spacings of the neutron-capture resonances for the even-odd isotopes. The capture cross sections have been measured recently by Browne and Berman[3]; the spin-state and spacing measurements are reported in this paper. The nuclear phase transition would be signaled most clearly by a change in the shape of the photonuclear giant resonance[2] (these measurements also have been carried out recently at Livermore[4]), but also might be indicated by an abnormal behavior of the spin-state distributions.

A previous measurement[5] indicated that the spin-state distribution of s-wave neutron resonances in (^{187}Os + n) might not be consistent with the usual $(2J+1)$ level-density distribution, which would imply an unusually small spin-cut-off factor for this nucleus. This measurement, however, was inconclusive, owing to the small mass and purity of the isotopically enriched sample available at the time, and the consequent large statistical uncertainties. A study of the spin-cut-off factors also could yield information on the nuclear shapes of these deformed nuclei. Thus it is worthwhile to reexamine and extend the spin-state measurements of the resonances in the osmium isotopes.

The general method is similar to that first reported by Wetzel and Thomas,[6] and used by two of us in previous work.[5,7] Both neutron times of flight and low-energy capture γ-ray pulse heights are recorded in a two-parameter experiment. The observed low-energy γ rays originate from low-lying states of the compound nucleus which are fed by cascade transitions originating from the capture (resonance) states. The ratio of selected γ-ray intensities is related to the spin of the capture state, so that these ratios should fall into two groups, corresponding to the two possible s-wave resonance spin values $J = I \pm \frac{1}{2}$. The method is based upon the simple idea that it is easier to reach a low-lying state via cascade transitions which involve a smaller total spin change than to reach a level requiring a larger spin change. Recently it has been shown[8] that in deformed nuclei, the populations of the low-lying levels also are influenced by the rotational band structure. Monte Carlo calculations[9] for these nuclei indicate that the ratio of the average values of the γ-ray intensity ratios for the two spin groups is expected to be 1.98 for (^{187}Os + n) and 1.75 for (^{189}Os + n).

II. EXPERIMENTAL PROCEDURE

The measurements reported here were performed at the Lawrence Livermore Laboratory 100-MeV Linac. Neutrons were produced when electron beam pulses struck a water-cooled tantalum target, which was aligned so that the col-

limated 17.3-m flight path viewed neutrons only from the water moderator. The electron beam parameters were as follows: 20-nsec pulse width, 720-sec^{-1} repetition rate, and 5-A peak pulse current.

In order to increase the count rate, two nearly identical 55-cm^3 Ge(Li) detectors were placed symmetrically about the capture target to detect γ rays at about 90° with respect to the neutron beam direction. The detectors were protected from neutron damage by slabs of ^{6}LiD 1.27 cm thick. A cadmium filter, 0.051 cm thick, was placed in the neutron beam to prevent very slow neutrons from overlapping in time with faster neutrons from the following beam pulse. In addition, lead filters, 0.64 cm thick for the ^{189}Os run and 1.27 cm thick for the ^{187}Os run, were placed in the neutron beam to reduce the effect of the γ flash produced when the electron beam strikes the tantalum target. (The flash saturates the preamplifiers and amplifiers so that useful data cannot be taken until these circuits recover fully.) To reduce this effect further, charge was injected into the preamplifier circuits to coincide with and partially cancel the flash pulses[10] (see Fig. 1). This was done for the ^{189}Os run but not for the ^{187}Os run, since the latter sample was much less massive and therefore scattered fewer of the flash γ rays into the detectors.

Isotopically enriched powdered metal samples were used. The ^{189}Os sample was in the shape of a disk, 0.64 cm thick and 3.81 cm in diameter, placed with its axis parallel to the neutron beam. Its mass was 30.94 g; it was enriched to 94.5% ^{189}Os, and contained only 0.1% ^{187}Os. The ^{187}Os sample was in the shape of a cylinder, 0.64 cm in diameter and 2.79 cm in height, placed with its axis perpendicular to the neutron beam. Its mass was 2.96 g; it was enriched to 70.96% ^{187}Os, and contained 5.09% ^{189}Os. Both samples also contained small amounts of even-even osmium isotopes. The neutron time of flight and γ-ray pulse height for each event were recorded on a magnetic drum in a two-dimensional array consisting of 1900 time-of-flight channels by 1020 pulse-height channels. The data-acquisition system consisted of PDP-8 and PDP-15 on-line computers, a time digitizer, and an analog-to-digital converter. Data later were transferred to magnetic tape for off-line analysis. A description of this data acquisition system has been given elsewhere.[11] A "time-crunching" software routine allowed the use of larger time-channel widths for the longer flight times, in order to conserve drum

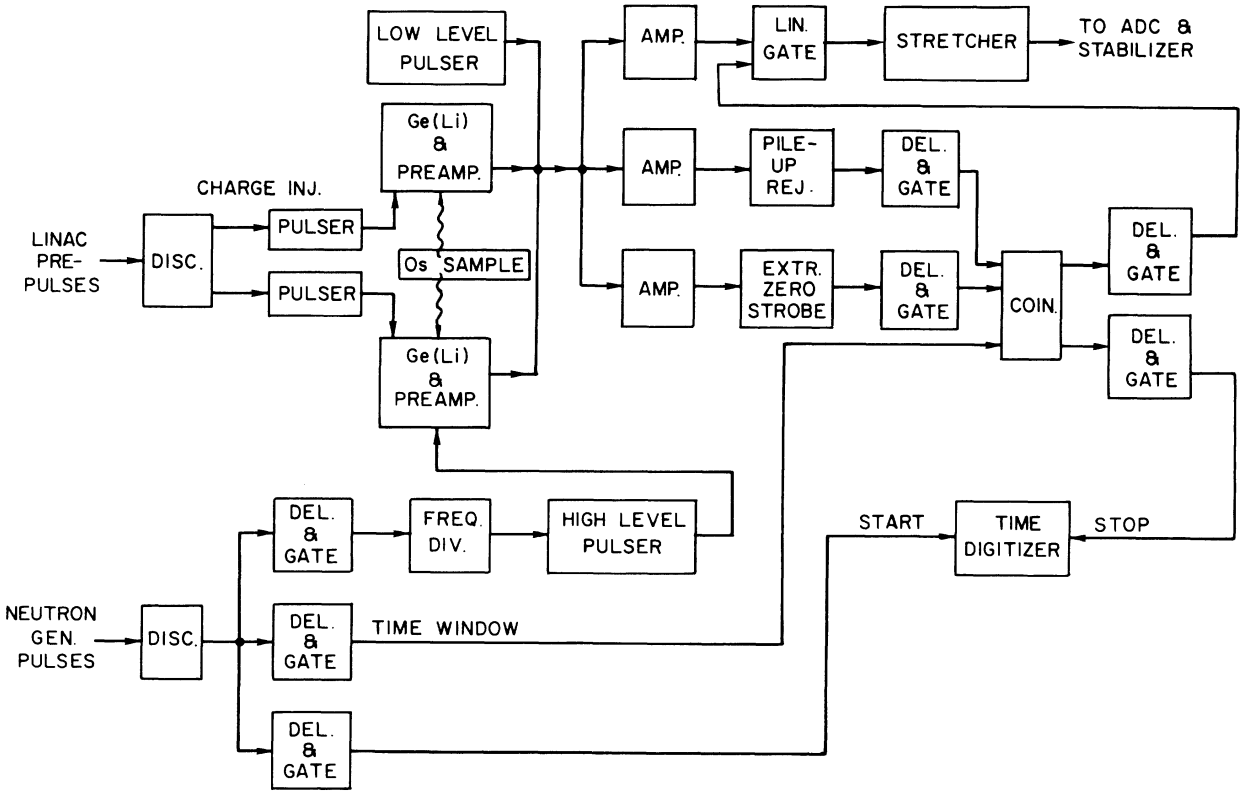

FIG. 1. Block diagram of the electronics for two-parameter (time-of-flight and pulse-height) data acquisition.

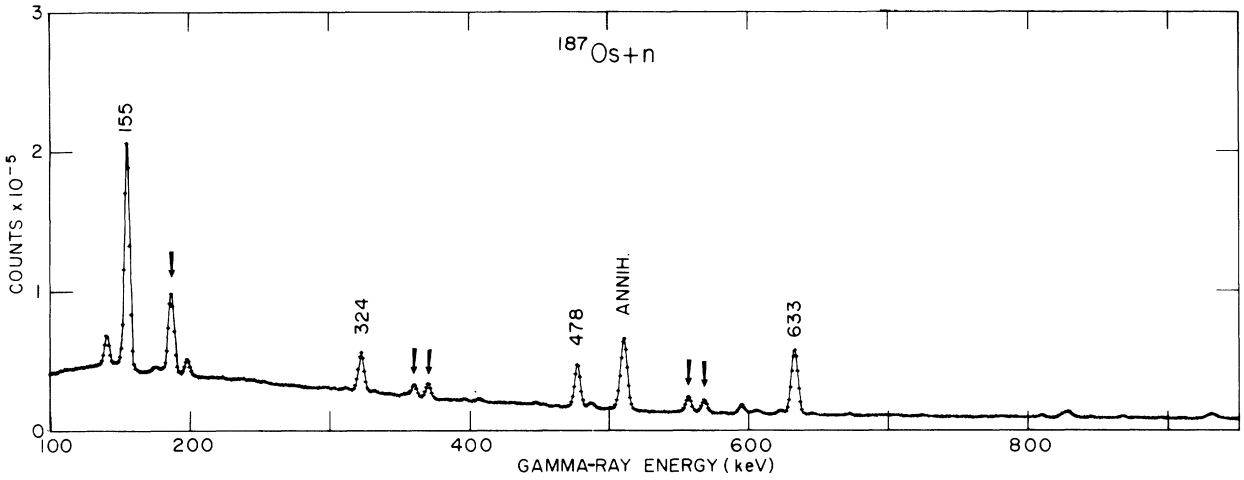

FIG. 2. Low-energy capture γ-ray spectrum for the ^{187}Os sample, integrated over all time-of-flight channels. γ rays from (^{187}Os+n) are labeled with their energies in keV. The arrows indicate capture γ rays from the ^{189}Os contaminant.

storage space without sacrificing resolution. The data tapes were analyzed to subtract background and to obtain the neutron time-of-flight spectra corresponding to particular γ rays as well as the γ-ray spectra corresponding to particular neutron resonances.

Signals from the two Ge(Li) detector preamplifiers were mixed, after the preamplifiers were adjusted carefully to have equal gain. In this way, the count rate was approximately twice that for a single detector, although there was some sacrifice in resolution. The resolution width for 1.33-MeV γ rays was about 3 keV, which was adequate for these measurements. The mixed signals then were split into three branches, as shown in Fig. 1. One branch was fed to the analog-to-digital converter (ADC) and stabilizer, another used an extrapolated zero strobe to provide the time digitizer with stop (event) pulses, and the third utilized a pile-up rejection circuit to gate the other branches. Gate and delay generators were used to set a time window to span the time region of interest and to prevent the counting of pulses during the first 24 μsec after the γ-flash. Low-level and high-level pulsers were used to provide references for a digital stabilizer in order to prevent long-term gain and zero-level drifts. The high-level pulser was triggered by a delayed gate pulse; this placed these standard pulses at the end of the time-of-flight region in order to avoid flash effects or any serious interference with the data.

III. TREATMENT OF THE DATA

The low-energy capture γ-ray spectrum for the ^{187}Os sample integrated over all time-of-flight channels is shown in Fig. 2. Figure 3 shows a

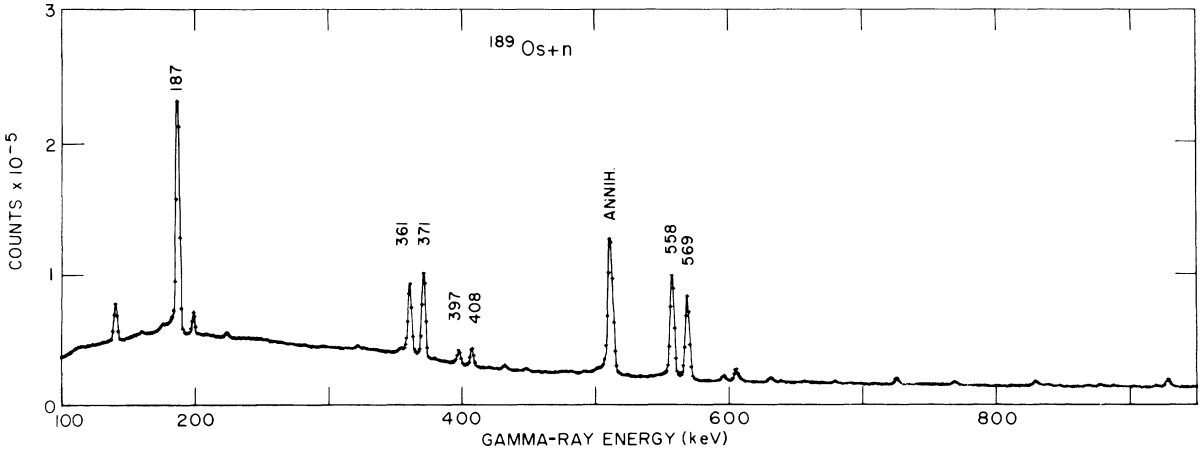

FIG. 3. Low-energy capture γ-ray spectrum for the ^{189}Os sample, integrated over all time-of-flight channels. γ rays from (^{189}Os+n) are labeled with their energies in keV.

TABLE I. Ratios of intensities of γ rays depopulating low-lying levels.

Target Nucleus	Possible Resonance Spins	Relevant Decay Scheme J^π keV	Lines Used In Ratio (keV)	Calculated Ratio
^{187}Os	$0^-, 1^-$	2^+ 633, 4^+ 479, 2^+ 155, 0^+ 0 — ^{188}Os	324/155	1.98 ± 0.30
^{189}Os	$1^-, 2^-$	4^+ 955.6, 3^+ 756.1, 2^+ 558.2, 4^+ 547.8, 2^+ 186.7, 0^+ 0 — ^{190}Os	361/187 397/187 408/187	1.75 ± 0.13

similar γ-ray spectrum for the ^{189}Os sample. The origins of the important γ-ray lines in these figures are shown in the relevant partial decay schemes[12,13] shown in Table I. The ratios of the intensities of γ rays which originate from 4^+ levels to those which originate from 2^+ levels yield the largest separation of the two resonance spin groups. These are given in the fourth column of the table. The last column gives the results of a Monte Carlo calculation[9] of the expected ratio of the average intensity ratios for the two spin groups; i.e., these values provide a measure of the expected separation of the spin groups.

The data were analyzed by obtaining the time-of-flight spectra corresponding to the low-energy γ rays of interest. Background correction was done by subtracting the time-of-flight spectra corresponding to regions on either side of the γ-ray peak. Figure 4 illustrates the time-of-flight spectrum for (^{187}Os + n) obtained in this way, corresponding to the 155-keV line. Since this line occurs only for the ^{187}Os isotope, all of the observed resonances result from neutron capture by this isotope.

A similar time-of-flight spectrum for (^{189}Os + n) is shown in Figs. 5(a) and 5(b), corresponding to the 187-keV γ ray. The spectrum shown in Fig. 5(c) is for the same neutron energy region as in Fig. 5(b), but these data correspond to the 361-keV γ ray. The comparison of the data in Figs. 5(b) and 5(c) illustrates two points: First, there are obvious differences in the relative sizes of some of the resonances, showing the effect of differences of the resonance spin; and second, the data in Fig. 5(c) clearly correspond to a thicker

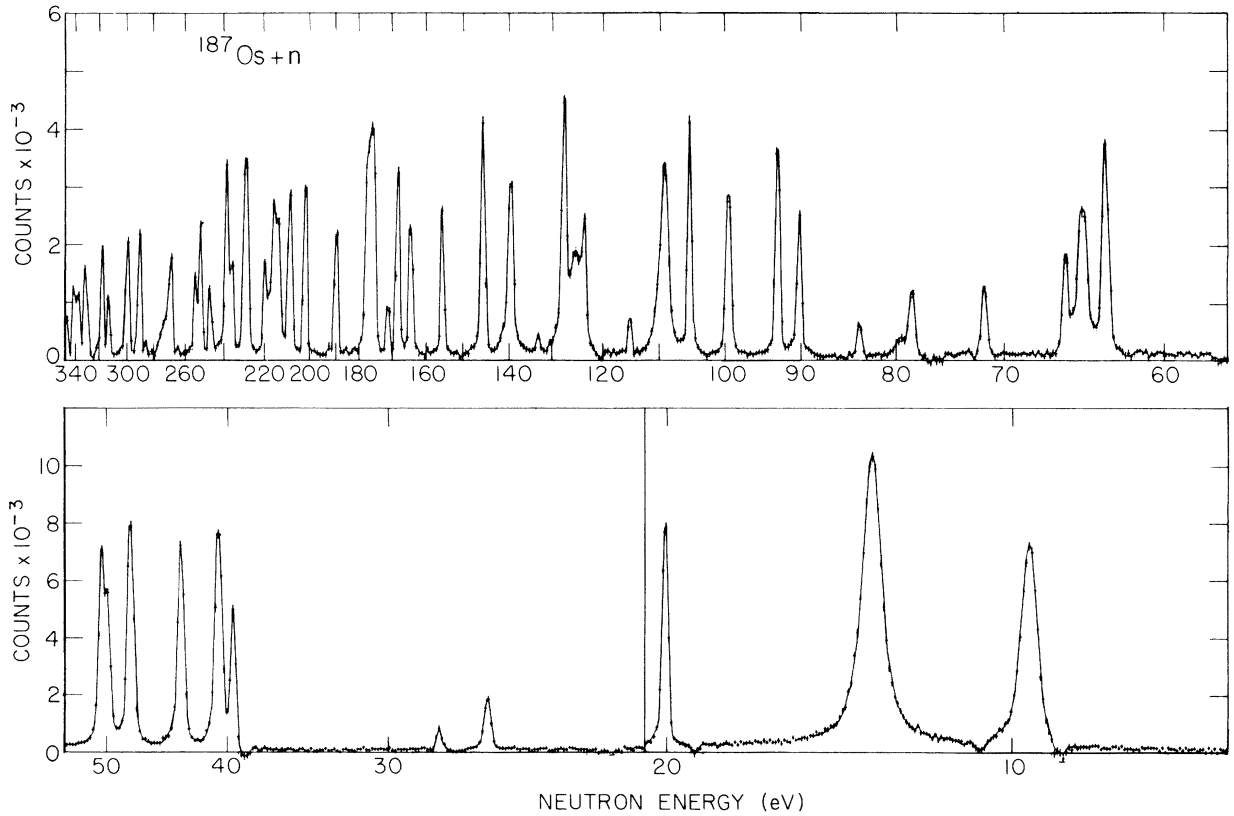

FIG. 4. Background-corrected time-of-flight spectrum for (^{187}Os + n) corresponding to the 155-keV γ ray. The three regions shown correspond to channel widths of 0.256, 0.512, and 1.024 μsec, in order of decreasing energy (increasing time of flight).

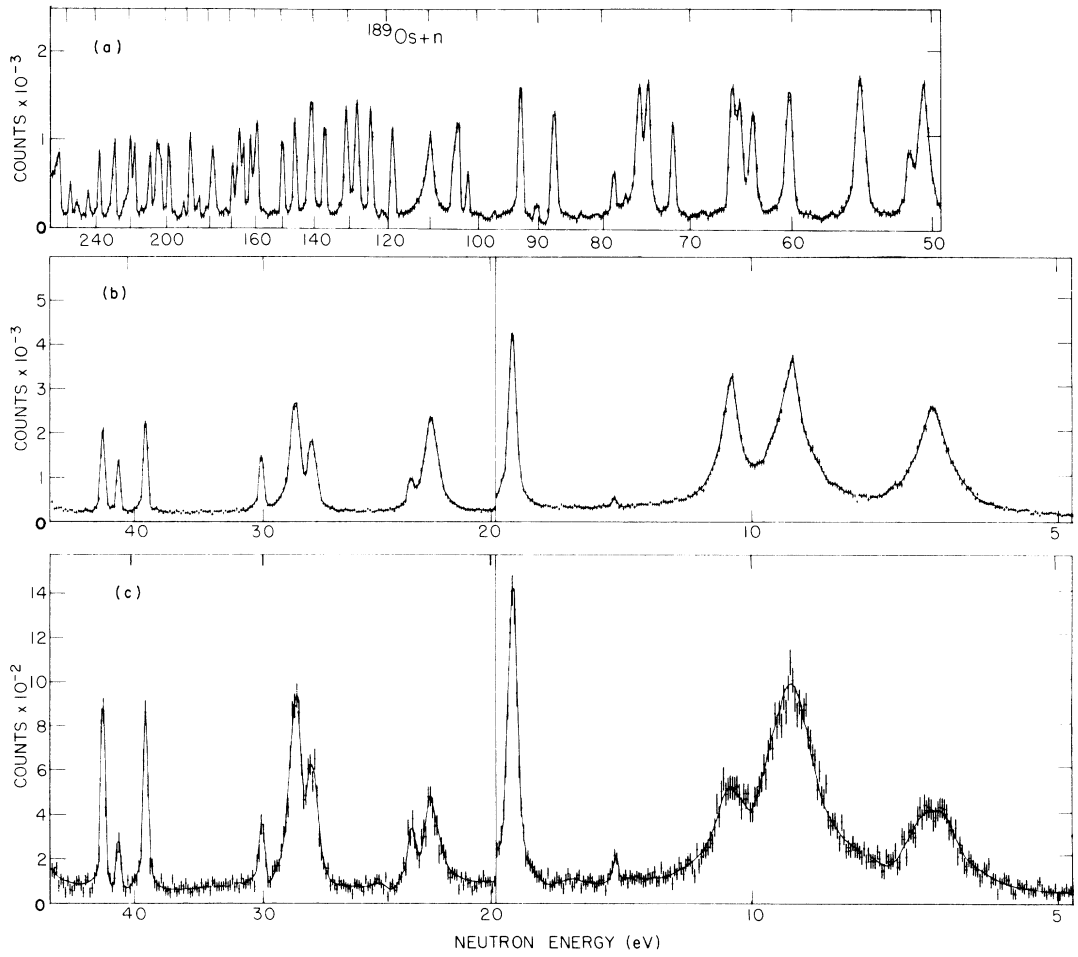

FIG. 5. Background-corrected time-of-flight spectrum for (^{189}Os+n). Curves (a) and (b) correspond to the 187-keV γ ray, with the channel widths as in Fig. 4. Curve (c) is for the same region as for curve (b), but these data correspond to the 361-keV γ ray.

sample than the data in Fig. 5(b), as can be seen from the shapes of the larger resonances. This results from the self-absorption effect on the capture γ rays; i.e., for the 187-keV data, it is mainly those γ rays which originate near the surface of the sample which are observed, whereas the observed 361-keV γ rays can originate from capture events which take place deeper within the sample. We must account for this change in effective sample thickness with γ-ray energy, at least for the larger resonances. The simplest way to do this is to avoid the central portions of the large resonances, and to use only the integrated intensity in the wings of the resonances in order to produce, in effect, a thin sample for both γ rays. This was done for all the large resonances (those below 50-eV neutron energy) for both isotopes. In those cases where two resonances overlap severely, we have used only the side of each resonance least affected by the presence of the other.

IV. RESULTS

A. ^{187}Os+n

For each resonance, the ratio of the intensity corresponding to the 324-keV transition (originating from a 4^+ level) to the 155-keV transition (from a 2^+ level) is formed. Figure 6 is a plot of these ratios vs neutron energy. A histogram of the distribution of these ratios, obtained as described in Ref. 5, is shown on the right. The ratios fall into two groups; the larger ratio corresponds to the larger capture-state spin ($J=1$). The error bars shown are the statistical uncertainties. The solid horizontal lines are the average values for each spin group, and the dashed lines show the extent of the Porter-Thomas type

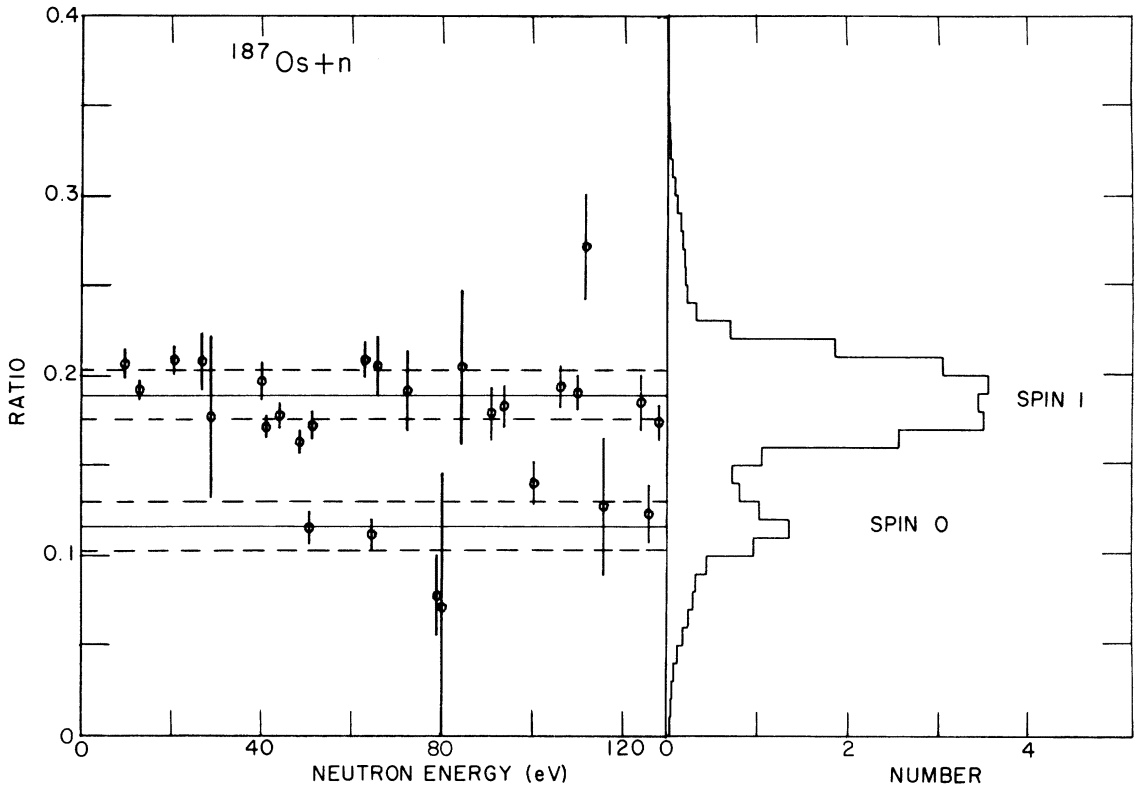

FIG. 6. The resonance intensity ratio corresponding to the 324-keV γ ray to the 155-keV γ ray vs resonance energy for (^{187}Os+n). A histogram of the distribution is shown on the right. The solid horizontal lines are the average values for each spin group, and the dashed lines show the extent of the Porter-Thomas type fluctuations.

fluctuations of the ratios obtained from the data. A full discussion of how these quantities were obtained has been given in previous publications.[5,7] The analysis has been limited to resonances below 128 eV, since at higher energies problems associated with poor resolution and the effects of the γ flash prevent us from making spin assignments with confidence.

Table II lists the resonances for neutrons captured by ^{187}Os, their assigned spin values, and

TABLE II. Spin assignments and their probabilities of correctness for resonances in (^{187}Os+n) with energies less than 128 eV, and observed resonance energies above this value.

Resonance energy (eV)	J	Probability (%)	Resonance energy (eV)	J	Probability (%)	Resonance energy (eV)	
9.5	1	100	71.4	1	99	129	211
12.7	1	100	78.0	0	99	131	213
20.2	1	100	79.5	(1) [a]	58	139	218
26.2	1	100	83.3	1	96	141	227
28.4	1	89	90.3	1	99	145	233
39.5	1	100	92.9	1	100	156	236
40.4	1	99	99.4	0	83	165	245
43.4	1	100	104.9	1	100	168	250
47.7	1	99	109.0	1	100	171	253
49.9	0	100	111.0			177	
50.7	1	99	114.8	(1)	55	179	
62.3	1	100	123.4	1	99	189	
63.9	0	100	124.9	0	98	201	
65.1	1	100	127.0	1	99	207	

[a] Assignment based partially upon a statistical test.

their probabilities of correctness, obtained as detailed in Refs. 5 and 7. For this purpose, a best fit for the *a priori* probabilities for the $J=1$ and $J=0$ resonances has been obtained from the data. No attempt was made to assign a spin to a small resonance at about 111 eV which is obscured by the resonance at 109 eV. Also listed are the energies of observed resonances above 128 eV, up to a region where about 20% of the resonances are being missed.

B. ^{189}Os+n

For (^{189}Os+n) there are three observed γ-ray lines which originate from 4^+ levels, corresponding to the 361-, 397-, and 408-keV transitions in ^{190}Os (see Table I). Although the levels with spin 4^+ at 548 and 956 keV belong to different rotational bands, they both are populated much less often[8] than the 187-keV level with spin 2^+. We therefore form the ratios of the resonance intensities corresponding to each of these γ rays to the 187-keV γ ray, and then combine these three ratios by weighting them inversely as the squares of their uncertainties. Figure 7 shows a plot of this combined ratio vs neutron energy. Again, the ratios fall into two groups and the larger ratio corresponds to the larger capture spin ($J=2$). (We have omitted from this plot the small resonances at 13.9, 78.0, 97.7, and 112.0 eV, which have very large uncertainties.) Based upon these ratios, we assign the spins and their probabilities of correctness; these are listed in Table III. Again, a best fit was found for the *a priori* probabilities for the two spin groups. Also listed are observed resonance energies above 170 eV, up to a region where about 20% of the levels are being missed.

All of the resonances which are listed in Tables II and III are assumed to result from the capture of s-wave neutrons. A test of this assumption was made for the small resonance in (^{189}Os+n) at 13.9 eV. From a comparison of the intensity of this resonance with resonances at 18.7, 21.9, 27.3, and 28.8 eV, for which the values for $2g\Gamma_n$ are known,[14] we obtain an estimate of $2g\Gamma_n$. Using estimated s- and p-wave strength functions for this mass region, we apply a Bayes' theorem analysis[15] to find that the probability that this resonance results from capture of p-wave neutrons is vanishingly small.

As a measure of the separation of the spin groups, we form the ratio of the average ratios shown in Figs. 6 and 7 to obtain 1.61 ± 0.03 and 1.94 ± 0.03 for (^{187}Os+n) and (^{189}Os+n), respectively. These are in reasonable agreement with the

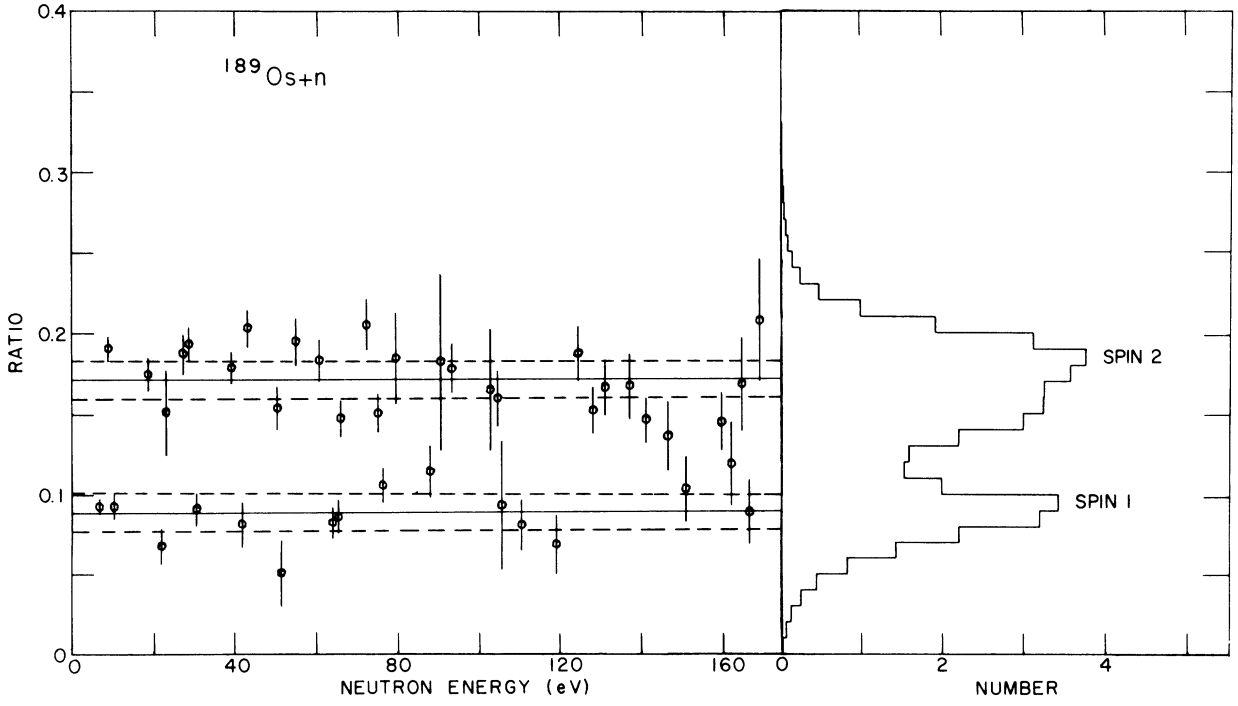

FIG. 7. Combined resonance intensity ratio corresponding to the 361-, 397-, and 408-keV γ rays to the 187-keV γ ray vs resonance energy for (^{189}Os+n). A histogram of the distribution is shown on the right. The horizontal lines have the same meanings as in Fig. 6.

TABLE III. Spin assignments and their probabilities of correctness for resonances in (^{189}Os + n) with energies less than 169 eV, and observed resonance energies above this value.

Resonance energy (eV)	J	Probability (%)	Resonance energy (eV)	J	Probability (%)	Resonance energy (eV)
6.71	1	100	79.5	2	99	178
8.95	2	100	87.9	1	96	183
10.3	1	100	90.6	2	87	188
13.9	(2) [a]		93.2	2	100	191
18.7	2	100	97.7			199
21.9	1	100	102.7	2	91	202
23.1	2	93	104.6	2	99	203
27.3	2	100	105.3	(1)	79	208
28.8	2	100	110.3	1	100	217
30.5	1	100	112.0			220
39.2	2	100	118.9	1	100	229
41.8	1	100	124.4	2	100	238
43.4	2	100	127.9	2	99	246
50.5	2	99	130.9	2	99	254
51.5	1	100	137.0	2	99	259
54.9	2	100	141.0	2	99	268
60.7	2	100	145.3	(2)	77	
64.0	1	100	150.8	1	98	
65.3	1	100	159.6	2	96	
66.0	2	99	162.0	(1)	69	
72.3	2	100	164.6	2	98	
75.2	2	99	166.3	1	99	
76.3	1	100	169.0	2	99	
78.0						

[a] Assignment based upon a statistical test.

results of the Monte Carlo calculations[9] given in Table I.

V. DISCUSSION

A. Distribution of spins

Using the probabilities of correctness listed in Tables II and III, the relative populations of the two spin groups and associated uncertainties were calculated using formulas (12) and (28) of Ref. 5, for both isotopes. These are given in the third column of Table IV. The ratio of these populations is given in the fourth column, which is to be compared with the ratio expected on the basis of a $(2J+1)$ level-density distribution given in the last column. Our observed spin distributions are seen to be compatible with a $(2J+1)$ distribution for both isotopes. This is contrary to the previous result[5] reported for (^{187}Os + n), where a deviation from a $(2J+1)$ distribution was indicated, which in turn implied an unusually small spin-cut-off factor. Indeed, the population ratio given in Table IV for (^{187}Os + n) is, if anything, on the high side of the value (3.0) expected for a $(2J+1)$ distribution, a result which certainly is not compatible with a small spin-cut-off factor. Since the nuclear moment of inertia is proportional to the square of the spin-cut-off factor,[16] the earlier result[5] would imply an unusual shape for the ^{188}Os compound nucleus. The results reported here, however, indicate that neither ^{188}Os nor ^{190}Os have shapes which are unusual for nuclei in this mass region for excitation energies near the neutron binding energy. The calculations of Ref. 2 predict a change in shape

TABLE IV. Relative resonance spin populations in (^{187}Os + n) and (^{189}Os + n).

Target nucleus	J	Relative spin populations (%)	Ratio of populations	Ratio from $(2J+1)$ distribution
^{187}Os	1	78.4 ± 5.0	3.63 ± 0.87	3.00
^{187}Os	0	21.6 ± 5.0		
^{189}Os	2	62.7 ± 4.5	1.68 ± 0.24	1.67
^{189}Os	1	37.3 ± 4.5		

from prolate for ^{188}Os to a γ-vibrational unstable configuration for ^{190}Os, based upon the low-lying excited states. Our results show no evidence for a major shape change, but it is not clear that the calculations are applicable to nuclear deformations at the much higher excitation energies (~8 MeV) characteristic of the neutron-resonance states populated in these experiments.

The spin distribution for (^{187}Os+n) is important in an astrophysical determination of the age of the universe based upon the β decay of ^{187}Re to ^{187}Os. This method depends upon the ability to separate the contribution of the radiogenic ^{187}Os from the ^{187}Os produced or destroyed by s-process (slow time scale) neutron capture in stars, which in turn requires the accurate measurement of these neutron-capture cross sections.[3] But in a star with $kT \simeq 30$ keV, both the ground state of ^{187}Os ($I^\pi = \frac{1}{2}^-$) and its first excited state at 9.8 keV ($I^\pi = \frac{3}{2}^-$) will be populated approximately equally. After s-wave neutron capture, they will form states in ^{188}Os with spins 0^- or 1^-, and 1^- or 2^-, respectively. Therefore, the important calculation of the capture cross section for the excited state requires a knowledge of the distribution and spacing of these spin states. Since we have shown that the spin distribution after capture by the ground state is consistent with a $(2J+1)$ distribution, and also that the spin distribution after capture by the ground state of ^{189}Os (where $I^\pi = \frac{3}{2}^-$) is as well, it can be inferred that the spin distribution after capture by the 9.8-keV excited state very likely also is consistent with a $(2J+1)$ distribution. This information reduces the uncertainty in the age of the universe obtained from the ^{187}Re $\rightarrow$ ^{187}Os dating technique.

B. Dyson-Mehta and uncorrelated Wigner statistics

Cumulative ("staircase") plots of the number of resonances vs neutron energy for (^{187}Os+n) and (^{189}Os+n) are shown in Figs. 8 and 9, respectively. They indicate that some levels are being missed above 150 eV for (^{187}Os+n), and above 120 eV for (^{189}Os+n). The mean-square deviation between such a staircase plot and a least-squares fitted straight line is the Dyson-Mehta Δ_3 statistic,[17] which can yield evidence for long-range ordering of the level spacings, assuming that there are no missing or spurious levels. Figure 10 indicates how values of Δ_3 calculated from the data vary as a function of the number of consecutive resonances included, for both compound nuclei. The shaded areas indicate the extent of the uncertainty limits for values for Δ_3 obtained from the Dyson-Mehta theory for a two-spin population (formulas 80, 81, and 82 of Ref. 17). It is seen that beyond a certain

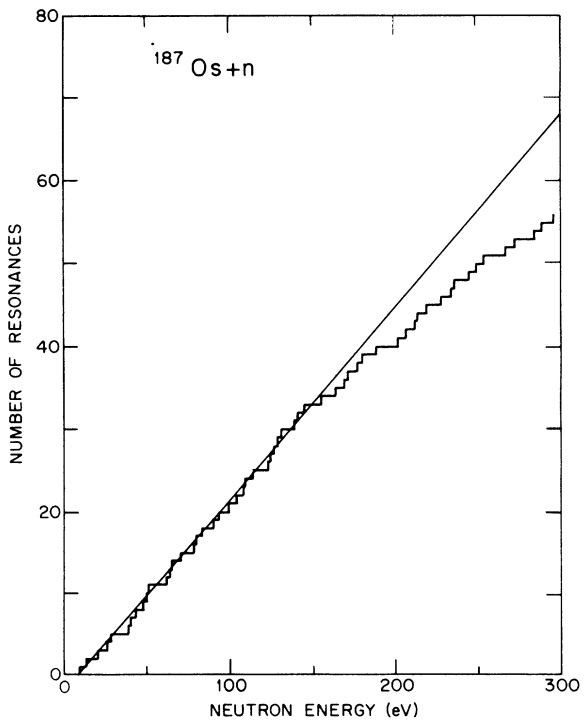

FIG. 8. Cumulative ("staircase") plot of the number of observed resonances vs neutron energy for (^{187}Os+n).

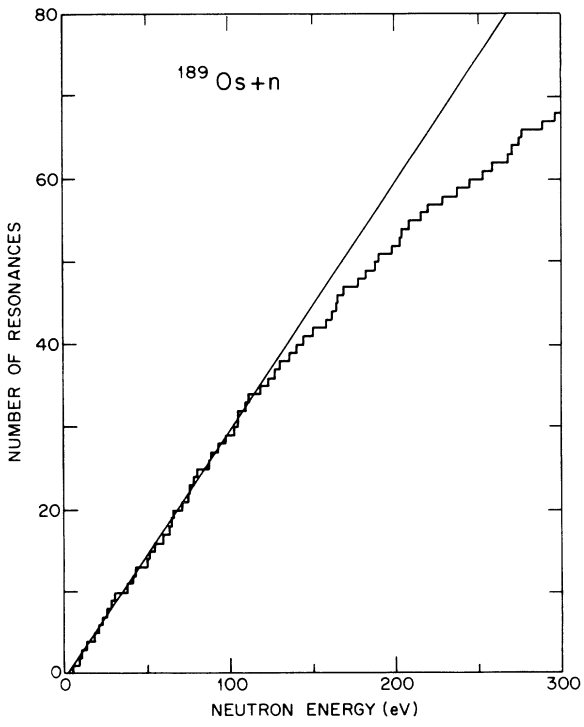

FIG. 9. Cumulative plot of the number of observed resonances vs neutron energy for (^{189}Os+n).

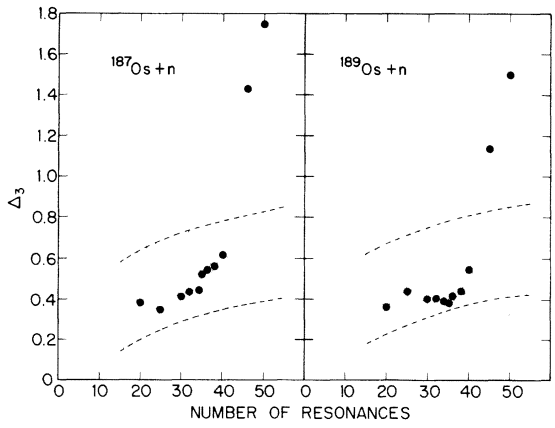

FIG. 10. Values for Δ_3 calculated from the data as a function of the number of consecutive resonances included for (^{187}Os+n) (left) and for (^{189}Os+n) (right). The shaded areas indicate the extent of the uncertainty limits for values for Δ_3 obtained from the Dyson-Mehta theory for a two-spin population.

point, values for Δ_3 increase rapidly, providing a sensitive test for missing resonances. Therefore, we have conservatively restricted our examination of the data for this purpose to the first 34 resonances for (^{187}Os+n) and to the first 35 resonances for (^{189}Os+n). The results are given in Table V. The values for Δ_3 obtained from the data are given in the third column, and the values calculated from the Dyson-Mehta theory for a two-spin population are given in the fourth column. The data agree reasonably well with the Dyson-Mehta theory, indicating that there probably are no missing resonances in this region, and that there is long-range ordering of the spacings; i.e., the series of resonances are spaced with a high degree of regularity, producing small values for Δ_3. The last column of Table V gives the results of a Monte Carlo calculation of the probability that an uncorrelated Wigner distribution of spacings yields values for Δ_3 smaller than those obtained from the data (third column). These probabilities are not small enough to reject the uncorrelated Wigner distribution definitely. [In these calculations, the two spin states were assumed to be mixed randomly, with populations proportional to $(2J+1)$.]

Since the Δ_3 statistic will increase if there are missing or spurious resonances in a consecutive series, it can be used, in principle, to test whether a particular resonance belongs to a given spin series. Table VI illustrates the effect on Δ_3 of including or omitting a small resonance of unknown spin from a consecutive series of resonances which are all of the same spin. It is seen that the 79.5-eV resonance in (^{187}Os+n) appears to belong to the $J=1$ series, since its inclusion produces a significantly smaller value for Δ_3, which agrees with the value obtained from the Dyson-Mehta theory (listed in the last column). For the case of the 13.9-eV resonance in (^{189}Os+n), the results indicate that it does *not* belong to the $J=1$ series, although the test with the $J=2$ series is inconclusive. Spin assignments for these two resonances, based upon these statistical tests, are included in Tables II and III.

C. Average level spacings

It is possible to take advantage of the fact that the data are compatible with the Dyson-Mehta theory to calculate the average level spacings with rather small uncertainties through use of the W statistic (formulas 27 and 32 of Ref. 17). Again, we restrict our examination of the data to the first 34 resonances in (^{187}Os+n) and to the first 35 resonances in (^{189}Os+n). In this way we obtain 4.42 ± 0.17 eV and 3.33 ± 0.12 eV for the average s-wave level spacings near the neutron separation energy in ^{188}Os and ^{190}Os, respectively. The corresponding values, obtained directly from the slopes of the staircase plots, are 4.30 ± 0.24 and 3.32 ± 0.18 eV, respectively. It should be noted that the value for the average level spacing for (^{187}Os+n) thus obtained also is needed for the astrophysical calculation described in Sec. V A.

D. Distribution of spacings

The solid histograms plotted in Fig. 11 show the distributions of the s-wave level spacings for the first 33 spacings for (^{187}Os+n) and for the first

TABLE V. The Dyson-Mehta Δ_3 statistic, and comparison with an uncorrelated Wigner distribution. The two possible spin states are assumed to be randomly mixed, with populations proportional to $(2J+1)$.

Target nucleus	Number of resonances	Δ_3 (data)	Δ_3 (Dyson-Mehta)	Probability (%) (Uncorrelated Wigner)
^{187}Os	34	0.44	0.53 ± 0.22	22.5 ± 2.8
^{189}Os	35	0.38	0.56 ± 0.22	9.4 ± 1.8

TABLE VI. Effect on Δ_3 of inclusion or omission of a resonance of unknown spin from a series of resonances of the same spin. The last two columns list values for Δ_3 obtained from the data and from the Dyson-Mehta theory for a single-spin population, respectively.

Target nucleus	Spin series (J)	Resonance status	Number of resonances	Δ_3 (Data)	Δ_3 (Dyson-Mehta)
^{187}Os	1	79.5 eV omitted	18	0.49	0.29 ± 0.11
^{187}Os	1	79.5 eV included	19	0.32	0.29 ± 0.11
^{189}Os	1	13.9 eV omitted	9	0.16	0.22 ± 0.11
^{189}Os	1	13.9 eV included	10	0.24	0.23 ± 0.11
^{189}Os	2	13.9 eV omitted	13	0.17	0.25 ± 0.11
^{189}Os	2	13.9 eV included	14	0.18	0.26 ± 0.11

34 spacings for (^{189}Os + n). The dashed histograms show the results of Monte Carlo calculations of the spacing distributions for a random mixture of two-spin populations, each of which follows a Wigner distribution, and with level densities proportional to $(2J+1)$. They are seen to fit the observed distributions reasonably well, even though there appear to be a few too many small spacings for the (^{187}Os + n) case.

E. Comparison with previous measurements

The spin assignments presented in this paper for resonances in (^{189}Os + n) are generally in good agreement with the results of Ref. 5, although there are disagreements for the 104.6-, 127.9-, and 159.6-eV resonances. Many new spin assignments have been made. For the case of (^{187}Os + n), the present data are superior to those of Ref. 5, so that the latter should be discarded. The poorer quality of the older data resulted primarily from the large statistical uncertainties caused by the relatively small mass and low purity of the isotopically enriched sample available at that time (0.30 g, 46% ^{187}Os). Also, the older assignments depended heavily upon multiplicity measurements, which have been shown[7,9] to yield a smaller separation of the spin groups than the method used in the present investigation. The superior sample available for these measurements (2.96 g, 71% ^{187}Os) and the more intense neutron pulses available from the Livermore linac have enabled us to obtain far better results, in which the spin groups are separated clearly.

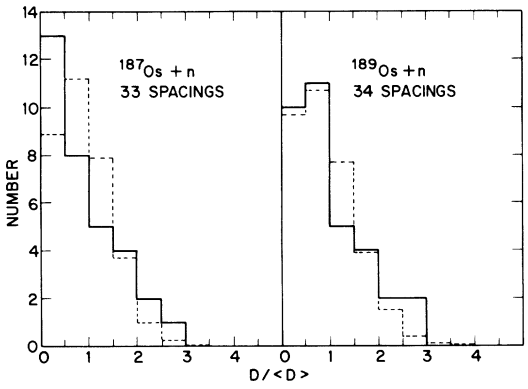

FIG. 11. Distributions of s-wave resonance spacings for (^{187}Os + n) (left) and for (^{189}Os + n) (right), represented by the ratio of the individual level spacings D to the average level spacing $\langle D \rangle$. The solid lines denote the observed data. The dashed lines show the results of Monte Carlo calculations of spacing distributions for a random mixture of two-spin populations with level densities proportional to $(2J+1)$, each of which follows a Wigner distribution.

VI. CONCLUSIONS

The spin states of 25 resonances populated by the capture of s-wave neutrons by ^{187}Os and 40 resonances for the case of ^{189}Os have been assigned with a probability of correctness greater than 80%. For both isotopes, the distribution of the spins has been found to be given well by a $(2J+1)$ level-density distribution. This information is necessary for the determination of the age of the universe by the ^{187}Re → ^{187}Os nuclear dating technique. At the same time, these results provide no evidence for a change in nuclear shape between ^{188}Os and ^{190}Os at excitation energies corresponding to the neutron resonances.

The level spacings for both isotopes have been shown to favor the theory of Dyson and Mehta, indicating the presence of long-range ordering. However, the data do not allow us to reject definitely an uncorrelated Wigner distribution.

ACKNOWLEDGMENTS

We wish to thank Dr. M. L. Stelts, Dr. J. C. Browne, and Dr. H. S. Camarda for their assistance at various stages of this investigation. One of us (A.S.) would like to express his appreciation for the hospitality accorded to him by the staff at the Livermore linac during his stay there.

†Work performed under the auspices of the U. S. Energy Research and Development Administration. W-7405-Eng-48.

*On sabbatical leave at Lawrence Livermore Laboratory (1974–1975).

[1]D. D. Clayton, Astrophys. J. 139, 637 (1964); S. E. Woosley (private communication).

[2]R. Sedlmayr, M. Sedlmayr, and W. Greiner, Nucl. Phys. A232, 465 (1974).

[3]J. C. Browne and B. L. Berman, Bull. Am. Phys. Soc. 20, 559 (1975); *ibid.* 20, 1508 (1975); Nature 262, 197 (1976).

[4]B. L Berman, D. D Faul, R. A. Alvarez, and P. Meyer (private communication).

[5]A. I. Namenson, A. Stolovy, and G. L. Smith, Nucl. Phys. A237, 45 (1975).

[6]K. J. Wetzel and G. E. Thomas, Phys. Rev. C 1, 1501 (1970).

[7]A. Stolovy, A. I. Namenson, J. C. Ritter, T. F. Godlove, and G. L. Smith, Phys. Rev. C 5, 2030 (1972).

[8]M. R. Macphail, R. F. Casten, and W. R. Kane, Bull. Am. Phys. Soc. 20, 97 (1975).

[9]A. I. Namenson, Nucl. Phys. A209, 252 (1973).

[10]M. L. Stelts and J. C. Browne, Nucl. Instrum. Methods 133, 35 (1976).

[11]G. T. Mattesich, in *Cube Symposium Proceedings* [CONF-741001, Lawrence Livermore Laboratory, 1974], p. 188.

[12]E. Bashandy and S. G. Hanna, Nucl. Phys. 84, 577 (1966).

[13]B. Harmatz and T. H. Handley, Nucl. Phys. 56, 1 (1964).

[14]H. E. Jackson and L. M. Bollinger, Phys. Rev. 124, 1142 (1961).

[15]L. M. Bollinger and G. E. Thomas, Phys. Rev. 171, 1293 (1968).

[16]T. Ericson, Adv. Phys. 9, 425 (1960).

[17]F. J. Dyson and M. L. Mehta, J. Math. Phys. 4, 701 (1963).